Hadronic Interaction Models and Cosmic Ray Composition

S. Ostapchenko[a,b*]
[a] *Institutt for fysikk, NTNU Trondheim, Norway*
[b] *D. V. Skobeltsyn Institute of Nuclear Physics, Moscow State University, Russia*

Abstract

An overview of hadronic interaction models, applied to extensive air shower simulations, is presented. The underlying model approaches are described in some detail, paying special attention to model treatment of high parton density regime. Differences in model predictions concerning basic air shower characteristics are analyzed and the relation of the latter to peculiar features of the models is investigated. Furthermore, model dependence of the cosmic ray composition determination is discussed in the context of present experimental situation, addressing in particular the puzzling results concerning the composition of ultra-high energy cosmic rays. Finally, the prospects for improving the situation with next generation of models are studied.

1 Introduction

Experimental studies of cosmic rays (CR) of very high energies are traditionally performed on the basis of extensive air shower (EAS) techniques. Thus, the information on the properties of primary CR particles - their energy, type, arrival direction - is inferred from the measured characteristics of air showers - huge nuclear-electro-magnetic cascades initiated by their interactions in the atmosphere. Correspondingly, the solution of the inverse problem, i.e., the determination of energy spectra and, especially, of particle composition of very high energy cosmic rays is impossible without a reliable description of EAS development, in particular, of its backbone - hadronic cascade. Consequently, the heart of any Monte Carlo (MC) EAS simulation program is the corresponding hadronic interaction generator employed, which is designed to reproduce correctly the properties of strong interactions relevant for air shower development.

To trace the connection between macroscopic features of hadron-nucleus (nucleus-nucleus) interactions and shower observables, let us remind that the two main techniques of EAS detection are based correspondingly on observations of fluorescence light, emitted from EAS cone by excited air molecules, and on measurements of charged particles, resulted from the EAS development, by ground-based arrays. In the former case, the energy of the incoming particle is estimated from the integrated amount of the fluorescence light emitted, while the basic measure of the CR composition is the so-called shower maximum position $X_{\rm max}$ - depth in the atmosphere (in g/cm^2), where maximal density of ionizing particles is produced. Using the second method, the energy spectrum and the composition of the primary cosmic radiation (PCR) are inferred from the measured densities of all charged particles and of muons correspondingly. Although the mentioned EAS characteristics depend non-trivially on various properties of hadronic interactions, for given energy of the primary particle the position of the shower maximum $X_{\rm max}$ is mainly defined by the inelastic (more precisely, non-diffractive) proton-air cross section and by the so-called inelasticity $K_{\rm inel}$ of p-air interactions. In turn, muon component of air showers

*e-mail: sergei@tf.phys.ntnu.no

grossly depends on the multiplicity of charged particles in pion-air interactions. Thus, when the fluorescence method is employed, the measured quantities are very sensitive to the interactions of the primary particle, whereas ground-based observables depend strongly on the development of the nuclear cascade in the atmosphere, which is dominated by interactions of secondary particles of energies much smaller than the one of the primary.

Hence, among the requirements to CR interaction models is their applicability to the description of general interactions of hadrons (typically, nucleons, charged pions, and kaons) with nuclei and nuclei with nuclei, reliable predictions for the corresponding total inelastic and diffractive cross sections, as well as for the inelasticity, and, most importantly, a significant predictive power of the corresponding underlying approach. The latter is dictated by the necessity to extrapolate such models over many energy decades - from the collider range, where the models can be calibrated, up to the highest CR energies.

In the following, we are going to discuss basic features of contemporary hadronic MC generators, used in the CR field, in connection to the corresponding predictions for EAS development and to present understanding of the PCR composition in the very high energy range.

2 Underlying picture

The underlying picture of high energy interactions is the one of multiple scattering processes, being mediated by numerous cascades of partons - quarks and gluons, developing between the interacting particles. It is important to keep in mind that such cascades develop in few dimensions: parton rapidity y_i, transverse momentum p_{t_i}, and transverse displacement b_i, the latter being related by the uncertainty principle to the parton virtuality: $b_i^2 \sim 1/q_i^2 \simeq 1/p_{t_i}^2$. One may consider few representative cases: purely "soft" cascades of low p_t partons, "hard" parton evolution with all the parton transverse momenta being large, and "semihard" cascades, which include both soft and hard partons.

In the first case, each new parton in the cascade is produced at a relatively large transverse distance $b_i \sim 1/p_{t_i}$ from its parent. Correspondingly, in such processes hadrons look big and grey, as depicted in Fig. 1 (a). Hadron size as viewed by a probe at rapidity distance Y is

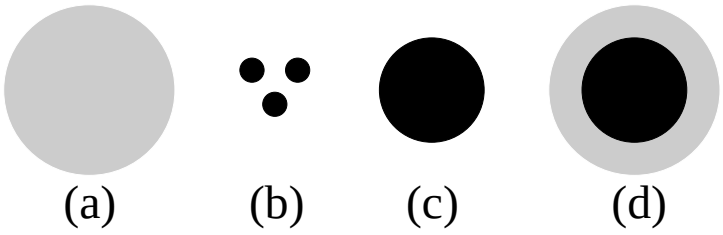

Figure 1: Hadron profile as viewed in soft (a), hard (b), semihard (c), and general (d) interactions.

$$R_h^2 \sim \langle n \rangle \, / \, \langle p_t^2 \rangle, \tag{1}$$

where the average number $\langle n \rangle$ of cascade steps is related to the typical rapidity distance between two subsequent parton emissions: $\langle n \rangle \sim Y \, / \, \langle y_{i+1} - y_i \rangle$. In turn, parton density can be estimated as

$$\rho_{g,q} \sim 2^{\langle n \rangle} \, / \, R_h^2 \sim \langle p_t^2 \rangle 2^{\langle n \rangle} \, / \, \langle n \rangle. \tag{2}$$

Here, one deals with processes characterized by large cross sections and relatively low parton densities, which give an important contribution at all interaction energies.

In the case of purely hard parton cascades, (1-2) gives high parton densities and low cross sections, a hadron looking like a number of black "hot spots", see Fig. 1 (b); the corresponding contribution to average (not triggered) interactions being negligible at all energies.

Finally, the dominant contribution to the semihard interactions is obtained in a two-step process: first, the cascade develops in the small p_t range, resulting in a fast parton diffusion towards large b; then, high p_t parton evolution becomes effective, leading to a quick rise of the parton density. Processes of that type, with hadrons looking both big and black, as shown in Fig. 1 (c), give the dominant contribution to very high energy interactions. However, general interactions involve all the mentioned cases; there is always a grey "nimb" around the black "core" - see Fig. 1 (d).

From the above discussion follows that high energy interaction models have to treat both soft and hard parton dynamics, and, when it comes to dealing with black regions of high parton density, have to address the corresponding high density effects, i.e. to account for nonlinear corrections to parton evolution.

3 Basic model approaches

Present model approaches to the treatment of high energy hadronic and nuclear collisions follow the logic proposed in the Quark-Gluon String Model [1] and Dual Parton Model [2], treating the interaction pattern as a superposition of a number of elementary rescattering processes corresponding to individual independent parton cascades. In that context, it is not generally necessary to describe the internal structure of such partial cascades in detail, rather it is sufficient to define the amplitude for an elementary scattering process and an effective hadronization procedure which allows to convert final s-channel partons into secondary hadrons, whereas the multiple scattering aspect is treated within the Gribov's Reggeon approach [3]. Thus, instead of describing hadron-hadron scattering amplitude by means of the diagrams of Fig. 2 (left), where individual parton cascades are depicted symbolically as ladders, one replaces each lad-

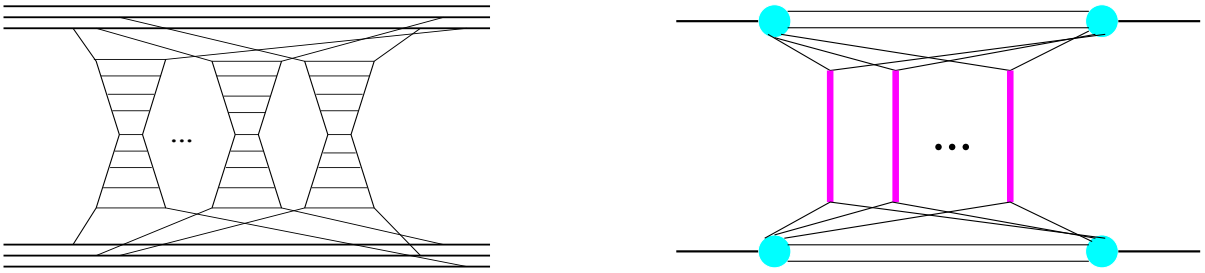

Figure 2: Left: general contribution to hadron-hadron scattering amplitude corresponds to multiple exchanges of parton ladders. Right: the same contribution is described by multiple Pomeron exchanges (vertical thick lines).

der by an effective object - Pomeron, whose internal structure is not important at that stage, hadron-hadron amplitude being expressed via the Pomeron exchange amplitude (Fig. 2 (right)).

The optical theorem allows one to obtain immediately the total cross section for the scattering, moreover, using the so-called Abramovskii-Gribov-Kancheli (AGK) cutting rules [4], one is able to derive partial contributions to the total cross section, corresponding to particular final state configurations. In doing so, one distinguishes elementary production processes, where final partons in the cascade loose their coherence and are converted in hadrons, and virtual (elastic) rescatterings, where all the partons after the scattering processes recombine back to their parent hadrons. Describing the former as "cut" and the latter as uncut Pomerons and summing over any number of unobservable virtual rescattering processes (uncut Pomeron exchanges),

one obtains, for example, usual (quasi-)eikonal expressions for the inelastic cross section and for partial contributions of inelastic interactions with precisely n elementary production processes (cut Pomerons):

$$\sigma_{ad}^{\rm inel}(s) = \int d^2b \sum_{j,k} C_a^{(j)} C_d^{(k)} \left(1 - e^{-2\,\lambda_a^{(j)}\,\lambda_d^{(k)}\,\chi_{ad}^{\mathbb{P}}(s,b)}\right) \tag{3}$$

$$\sigma_{ad}^{(n)}(s) = \int d^2b \sum_{j,k} C_a^{(j)} C_d^{(k)} \frac{\left[2\,\lambda_a^{(j)}\,\lambda_d^{(k)}\,\chi_{ad}^{\mathbb{P}}(s,b)\right]^n}{n!} e^{-2\,\lambda_a^{(j)}\,\lambda_d^{(k)}\,\chi_{ad}^{\mathbb{P}}(s,b)} \tag{4}$$

where the eikonal $\chi_{ad}^{\mathbb{P}}(s,b)$ is the imaginary part of the Pomeron exchange amplitude in the impact parameter representation and $C_a^{(j)}$, $\lambda_a^{(j)}$ are correspondingly relative weights and relative strengths of elastic scattering eigenstates for hadron a.

Thus, typical procedure for simulating hadronic interactions starts from sampling the number n of elementary production processes according to cross sections $\sigma_{ad}^{(n)}$ (or sampling a diffraction interaction according to the corresponding cross section), performs energy-momentum sharing between those processes, and treats secondary particle production by means of the corresponding hadronization procedure for each process separately.

Here, for purely soft (nonperturbative) parton cascades one usually employs the standard parametrization for the Pomeron eikonal [1], characterized by a power-like dependence on the c.m. energy squared s and by a Gaussian shape in impact parameter b:

$$\chi_{ad}^{\mathbb{P}_{\rm soft}}(s,b) \sim s^{\alpha_{\mathbb{P}}(0)-1}\ \exp\left[-\frac{b^2}{4(R_{ad}^2 + \alpha'_{\mathbb{P}}(0)\ \ln s)}\right], \tag{5}$$

$\alpha_{\mathbb{P}}(0)$ and $\alpha'_{\mathbb{P}}(0)$ being the intercept and the slope of the Pomeron Regge trajectory. Hadronization procedure is described in that case as a formation and break-up of strings of color field stretched between parton constituents of the projectile and target hadrons [1, 2].

In case of semihard processes, the procedure employed in the QGSJET [5], QGSJET-II [6], and EPOS [7] models is based on an introduction of some parton virtuality cutoff Q_0^2, which separates soft (all parton virtualities $q_i^2 < Q_0^2$) and hard ($q_i^2 > Q_0^2$) parton evolution, and treating the former by means of the soft Pomeron eikonal $\chi^{\mathbb{P}_{\rm soft}}$, while describing the latter within the DGLAP formalism. This way one obtains the so-called "semihard Pomeron" contribution, depicted in Fig. 3, corresponding to a piece of QCD parton ladder being sandwiched between two

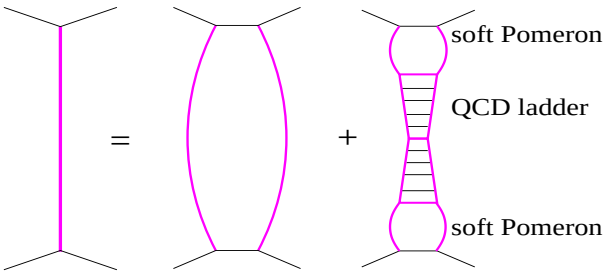

Figure 3: A "general Pomeron" (l.h.s.) consists of the soft Pomeron and the "semihard Pomeron" - correspondingly the first and the second contributions on the r.h.s.

soft Pomerons [8], such that a hard parton cascade is always preceded by a "soft pre-evolution", the latter being treated as soft Pomeron emission. This mimics precisely the dynamics described in the preceding Section: during the "soft pre-evolution" partons quickly diffuse towards the periphery (due to the finite slope of the Pomeron trajectory $\alpha'_{\mathbb{P}}(0)$), while hard parton branchings result in a quick rise of the parton density. Hadron production procedure includes in that

case an explicit simulation of the QCD parton cascade, such that strings of color field are stretched between parton constituents of the interacting hadrons and final s-channel partons from the QCD cascade. General elementary scattering process is then described as an exchange of a "general Pomeron", which is just the sum of the two contributions, with the eikonal $\chi_{ad}^{\mathbb{P}} = \chi_{ad}^{\mathbb{P}_{\rm soft}} + \chi_{ad}^{\mathbb{P}_{\rm sh}}$.

On the other hand, the SIBYLL model [9] is based on the minijet approach [10], which is qualitatively similar to the one described above, with an important difference that the soft cascade contribution ($q_i^2 < Q_0^2$) is neglected, a semihard process being described by the DGLAP ladder along, without the "soft pre-evolution". The justification for such a procedure is provided by identifying the cutoff Q_0^2 with an effective parton density "saturation scale" and neglecting parton (hence, hadron) production in the saturation regime, as discussed in the next Section.

Apart from the general framework described above, significant differences between existing models come from particular implementations of the basic algorithms, e.g., concerning energy-momentum partition between elementary production processes, string hadronization procedures, treatment of hadronic leading clusters which are left after cut Pomeron emissions.

4 Nonlinear effects

Crucial differences between present hadronic MC generators are related to how they treat nonlinear interaction corrections emerging in the high parton density regime. As discussed in the Introduction, in the very high energy limit the black region of high parton density is significantly extended towards moderately large impact parameters, such that "central" hadron-hadron (-nucleus) collisions constitute a significant fraction of the inelastic cross section. There, numerous parton cascades develop in parallel, being closely packed in the interaction volume, and start to overlap and to influence each other. In the QCD framework, the corresponding dynamics is described as merging of parton ladders, leading to the saturation picture: at a given virtuality scale parton density can not exceed certain value; going to smaller momentum fractions x, new parton splittings are compensated by merging of parton cascades [11].

In MC generators, one usually attempts to mimic the saturation picture in a phenomenological way. Standard procedure, employed for example in the SIBYLL model, is to treat the virtuality cutoff scale Q_0^2 as an effective energy-dependent saturation scale: $Q_0^2 = Q_{\rm sat}^2(s)$ and to neglect parton evolution (and hadron production) at $q^2 < Q_0^2(s)$. The parameters of the corresponding $Q_0^2(s)$ parametrization are usually tuned together with the other model parameters by fitting the measured proton-proton cross section.

A more sophisticated procedure has been employed in the EPOS model, where effective saturation effects are described by a set of parameters, such that corresponding parametrizations depend on energy, impact parameter, types of interacting hadrons, and of nuclear mass numbers in case of collisions involving nuclei. The corresponding mechanism influences not only the configuration of the interaction (how many processes of what type occur) but also energy partition between multiple processes and the hadronization procedure, the relevant parameters being fitted both with cross section and with particle production data. In particular, the hadronization of the region of high parton density is treated using the apparatus of the hydrodynamics.

Apart from serious conceptual drawbacks of such approaches, their main "pragmatic" disadvantage stems from the fact that model predictions in the very high energy limit are driven by the chosen parametrizations, whereas other, more theoretically motivated, model ingredients play a secondary role. Thus, the predictive power of the corresponding models is significantly degraded. An alternative approach has been employed in the QGSJET-II model, providing a dynamical microscopic treatment of nonlinear interaction effects in the Reggeon framework: describing the latter by means of so-called enhanced Pomeron diagrams [12], corresponding to Pomeron-Pomeron interactions, some examples shown in Fig. 4. In particular, the procedure proposed in [13] allowed to resum the contributions of general "net"-type enhanced diagrams

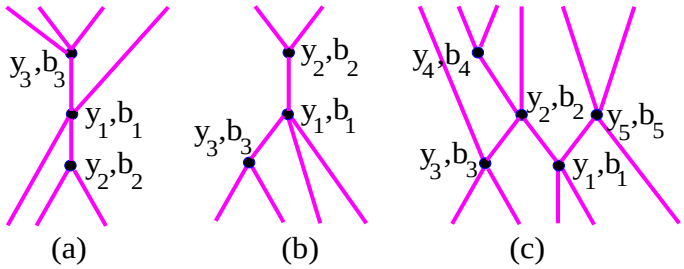

Figure 4: Examples of enhanced Pomeron diagrams.

to hadron-hadron (-nucleus) scattering amplitude to all orders in the triple-Pomeron coupling. Furthermore, to treat secondary particle production, the unitarity cuts of the corresponding diagrams have been analyzed and a procedure has been worked out to resum the corresponding contributions for any particular final state of interest [14]. The corresponding results have been obtained in the form of recursive equations which allowed one to implement the algorithm in the MC generator and to sample various configurations of the interaction in an iterative fashion. The approach proved to be powerful enough to describe consistently a great variety of experimental data on hadronic and nuclear collisions, while preserving the predictive power of the scheme; compared to the purely linear treatment of the original QGSJET model, there are only two additional parameters in QGSJET-II, which describe the structure of multi-Pomeron vertexes.

It is worth mentioning, however, that the discussed approach is based on the assumption that Pomeron-Pomeron coupling is dominated by soft ($q^2 < Q_0^2$) parton processes. Thus, the model has no dynamical evolution of the saturation scale: parton saturation may only be reached at the Q_0^2 scale; at $q^2 > Q_0^2$ parton evolution is described by purely linear DGLAP formalism.

5 Model dependence of cosmic ray composition

As discussed in the Introduction, model predictions for basic air shower observables grossly depend on the corresponding results for general characteristics of hadron-air collisions: inelastic cross section, inelasticity, charged particle multiplicity. The predicted proton-air cross section, plotted in Fig. 5, depends both on the model treatment and on the calibration to the data

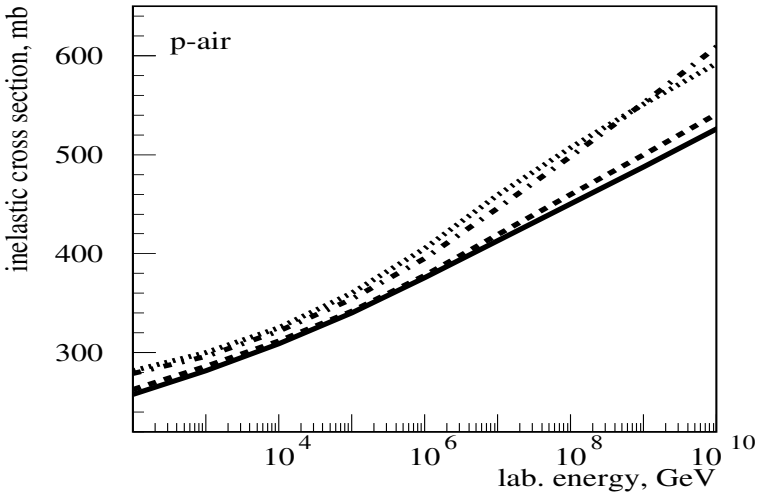

Figure 5: Model predictions for proton-air inelastic cross section: QGSJET - solid, QGSJET-II - dashed, SIBYLL - dot-dashed, and EPOS - dotted lines.

on proton-proton total cross section and elastic scattering slope. The results appear to be very similar between QGSJET and QGSJET-II, whereas SIBYLL and EPOS predictions are systematically higher, starting already from fixed-target energies, which is mainly due to the fact that inelastic screening corrections are not taken into account in those models. Both proton-air inelasticity and $N^{\rm ch}_{\pi-{\rm air}}$ in QGSJET-II are reduced by the nonlinear screening effects, compared to the original QGSJET, while the corresponding SIBYLL results are even lower, which is both because of neglecting the "soft pre-evolution" (parton production at $q^2 < Q_0^2$) in the minijet approach and due to the chosen parametrization of the energy-dependent virtuality cutoff $Q_0^2(s)$ (effective "saturation scale" of the model). Finally, EPOS results for $N^{\rm ch}_{\pi-{\rm air}}$ are similar to the ones of QGSJET up to 10^8 GeV lab. energy, whereas $K^{\rm inel}_{p-{\rm air}}$ appears to be the highest between all the models up to approximately 10^7 GeV and the smallest one above that energy, the predictions being driven by the effective saturation treatment of the model.

The discussed results project themselves on the model predictions for the shower maximum depth $X_{\rm max}$ and muon content at sea level N_μ, as plotted in Fig. 6. Due to the suppression

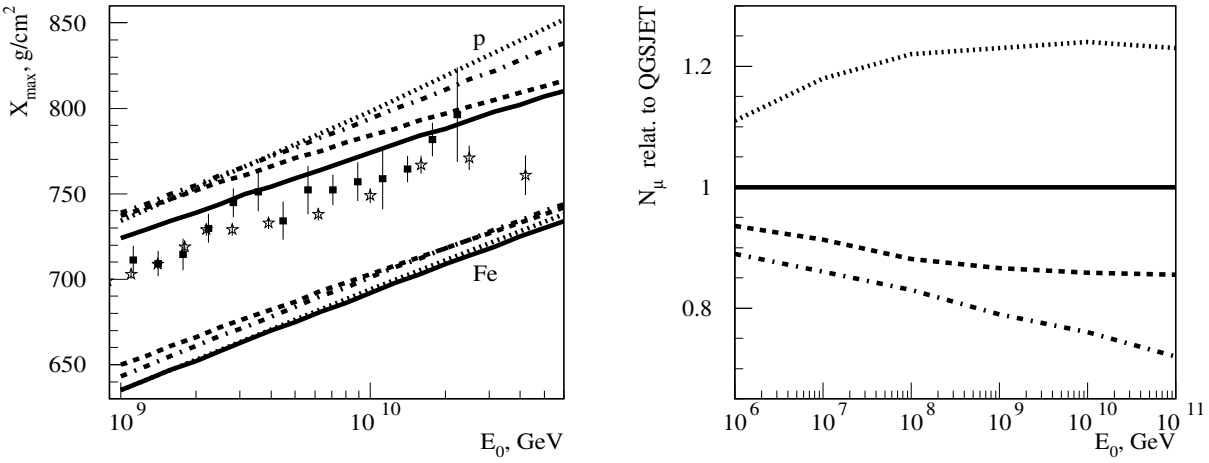

Figure 6: Left: model predictions for the EAS maximum depth, compared to data of HiRes (squares) [18] and Pierre Auger (stars) [19] Collaborations. Right: model predictions for N_μ in p-induced EAS at sea level (relative to QGSJET results). Abbreviations for the lines are the same as in Fig. 5.

of $K^{\rm inel}_{p-{\rm air}}$ and $N^{\rm ch}_{\pi-{\rm air}}$ in QGSJET-II, the predicted $X_{\rm max}$ is shifted deeper in the atmosphere and N_μ is reduced, compared to the original QGSJET. In case of SIBYLL and EPOS, the predicted $X_{\rm max}$ is driven by a competition between relatively high inelastic cross section and smaller inelasticity, compared to the two above-mentioned models. In the very high energy limit, the second effect seems to dominate the evolution of the shower maximum position which then goes noticeably deeper in the atmosphere. Concerning the predicted EAS muon content, the SIBYLL model, as expected, provides the smallest values between all the models, whereas the N_μ result of EPOS looks very surprising, exceeding the one of QGSJET-II at the highest energies by 40%. This is connected to the fact that the hadronization procedure, employed in that model, results in a significant enhancement of secondary (anti-)baryon production at high energies and in extremely hard spectra of secondary mesons in proton-nucleus collisions of very high energies [15]. The importance of (anti-)nucleon production for the EAS muon content has been pointed out long ago [16]: unlike pions and kaons, nucleons do not decay when reaching relatively low energies in the nuclear cascade; instead they continue to interact producing new generations of secondary particles. The role of harder spectra of secondaries can also be illustrated in a simple way: in a number of collisions, a very high energy charged pion may be produced; then, a single air shower is replaced by a pair of EAS, originating from

equally high energy particles (the leading secondary nucleon and the hard pion), the picture resembling the one for a nucleus-induced air shower.

How are these results reflected in the cosmic ray composition determined by modern CR experiments? The reference composition results in the "knee" region of the CR spectrum ($10^{15} \div 10^{16}$ eV) have been obtained by the KASCADE Collaboration, studying EAS electron-muon number correlations [17]. Both QGSJET and SIBYLL models behaved reasonably well in comparison with data, apart from certain discrepancies reported, and provided composition results which are qualitatively consistent with each other: the "knee" is caused by the steepening of the spectra of light elements (p and He) and the relative energy positions of partial spectral breaks appear to be rigidity-dependent (proportional to the respective charges of the primary nuclei), at least, for proton and helium components. It is also very remarkable that, despite certain model dependence of the obtained partial spectra of CR mass groups, the spectra of the proton component match well the corresponding results of direct (balloon) experiments. For QGSJET-II, the results are intermediate between the two cases above and, remarkably, the model appears to be consistent with preliminary data of the KASCADE-Grande Collaboration on the $N_\mu(N_e)$ dependence, which extend up to 10^{18} eV primary particle energies [20].

However, the situation with the PCR composition in the ultra-high energy range is much less clear. It is evident from Fig. 6 (right) that determining the CR composition on the basis of $X_{\max}$ data one obtains a model-dependent result, apart from a nonperfect agreement between the data of the HiRes and Pierre Auger Collaborations. Comparing HiRes data to $X_{\max}$ predictions of QGSJET and, to some extent, QGSJET-II, one arrives to a proton-dominated PCR composition in the energy range above 10^{18} eV, which is precisely the situation expected in the dip scenario for the transition between galactic and extragalactic CR components [21]. However, adopting the results of the two other interaction models and comparing with the Pierre Auger data, one obtains a composition which is a mixture of both light and heavy nuclei and which becomes gradually heavier with energy.

As has been demonstrated in [22], an independent cross-check of the composition results can be performed comparing the width (r.m.s.) $\sigma_{X_{\max}}$ of the distribution of measured shower maximum positions with the corresponding MC simulation results for a given primary composition. The power of that method is due to the fact that predicted $X_{\max}$ fluctuations demonstrate a very small dependence on the hadronic interaction model employed, while being very sensitive to the mass of the primary CR particle. In particular, it has been shown that the width of the $X_{\max}$ distribution for primary energies in excess of 10^{18} eV, measured by the HiRes Collaboration in the stereo mode, agrees perfectly well with the one predicted by models for the case of purely proton primaries. It is interesting to see if forthcoming Pierre Auger results on $X_{\max}$ distributions support these conclusions or, on the contrary, point towards a mixed / heavy-dominated PCR composition in the ultra-high energy range.

One of the significant advantages of the Pierre Auger Observatory is the possibility to study CR-induced EAS using both fluorescence and ground-based techniques and to compare corresponding composition results. In particular, such a comparison can be used as a consistency check for hadronic interaction models employed in the analysis. The first result of the kind appeared to be very striking, pointing on a much higher EAS muon content than predicted by the models: by more than 60% if compared to QGSJET-II predictions for proton-induced air showers, the conclusion being confirmed by three independent, although indirect methods [23]. None of the present models, with a possible exception of EPOS, seems to be compatible with that finding, even if one assumes that primary cosmic rays are iron nuclei above 10^{18} eV.

6 Future progress

Further improvements of the CR interaction models are presently in progress. In particular, the final step of the QGSJET-II development is aimed on the treatment of an additional class

of enhanced Pomeron diagrams - so-called "Pomeron loop" contributions, which contain multi-Pomeron vertices, connected to each other by two or more Pomerons, and which have been so far neglected in the scheme. Though such contributions are suppressed in central collisions by exponential factors, they provide finite screening corrections at moderately large impact parameters and require to chose a somewhat smaller value for the triple-Pomeron coupling, compared to the presently used value, in order to be consistent with data on $\sigma_{pp}^{\rm tot}(s)$. This leads, first, to a reduction of high mass diffraction in hadronic interactions at very high energies, secondly, to smaller screening effects in hadron-nucleus and nucleus-nucleus collisions, where the relative contribution of central (high density) to peripheral interactions is higher than in hadron-proton case. Hence, calibrating the model to the same hadron-proton data, one obtains higher inelasticity and charged particle multiplicity for hadron-air interactions, which will lead to a shift of the predicted $X_{\rm max}$ higher in the atmosphere and will result in a somewhat higher EAS muon number. However, both effects are expected to be very moderate; the resulting model predictions should stay between the ones of the present QGSJET-II and QGSJET models.

It is worth discussing if significant changes of EAS muon content can be expected when one takes a more full advantage of the present progress in the low x QCD, e.g., within the so-called Color Glass Condensate framework [24]. One possible modification may come from replacing the DGLAP description of hard parton evolution by the BFKL one, which would lead to a quicker rise of the parton density, hence, of the multiplicity of secondary particles and, in turn, of the EAS muon number. However, next-to-leading order BFKL evolution proved to be rather similar to the DGLAP case over relatively short parton rapidity intervals. On the other hand, in the very small x (large y) regime, one arrives to a high parton density, where saturation effects start to dominate secondary particle production. Thus, the potential N_μ enhancement can only be moderate in that case. More important should be a dynamical treatment of the saturation effects for relatively high parton virtualities. In the QGSJET-II model, parton saturation may only be reached below the virtuality cutoff scale Q_0^2; above that cutoff parton density rise is governed by the purely linear DGLAP evolution. Additional screening and saturation effects for $q^2 > Q_0^2$ should lead to a suppression of the average parton density, hence, to a reduction of the N_μ predicted. However, if the scheme allows one to reach a higher parton density *in the saturation regime* and/or to obtain a quicker expansion of the high parton density regime towards large impact parameters, one may achieve a very significant enhancement of secondary particle multiplicity, hence, of EAS muon content.

Acknowledgments

The author would like to thank the Organizing Committee of the Workshop for the invitation and to acknowledge the support of the European Commission under the Marie Curie Intra-European Fellowship Programme (project MC/IEF/C2CR/220251).

References

[1] A. B. Kaidalov and K. A. Ter-Martirosian, Phys. Lett. **B117**, 247 (1982).

[2] A. Capella *et al.*, Phys. Rep. **236**, 225 (1994).

[3] V. N. Gribov, Sov. Phys. JETP **26** (1968) 414; **29** (1969) 483.

[4] V. A. Abramovskii, V. N. Gribov, and O. V. Kancheli, Sov. J. Nucl. Phys. **18** (1974) 308.

[5] N. N. Kalmykov, S. S. Ostapchenko, and A. I. Pavlov, Bull. Russ. Acad. Sci. Phys. **58** (1994) 1966; Nucl. Phys. Proc. Suppl. **52B** (1997) 17.

[6] S. Ostapchenko, Nucl. Phys. Proc. Suppl. **151** (2006) 143; Phys. Rev. D **74**, 014026 (2006); AIP Conf. Proc. **928** (2007) 118.

[7] K. Werner, F.-M. Liu and T. Pierog, Phys. Rev. C **74**, 044902 (2006).

[8] H. J. Drescher *et al.*, J. Phys. G: Nucl. Part. Phys. **25** (1999) L91; S. Ostapchenko *et al.*, J. Phys. G: Nucl. Part. Phys. **28** (2002) 2597.

[9] R. S. Fletcher *et al.*, Phys. Rev. D **50** (1994) 5710; R. Engel *et al.*, Proc. of 26-th Int. Cosmic Ray Conf. (Salt Lake City), v. 1, p. 415, 1999.

[10] L. Durand and P. Hong, Phys. Rev. Lett. **58** (1987) 303; H. N. Wang, Phys. Rep. **280** (1997) 287.

[11] L. Gribov, E. Levin, and M. Ryskin, Phys. Rep. **100** (1983) 1.

[12] J. L. Cardi, Nucl. Phys. **B75** (1974) 413; A. B. Kaidalov, L. A. Ponomarev, and K. A. Ter-Martirosyan, Sov. J. Nucl. Phys. **44** (1986) 468.

[13] S. Ostapchenko, Phys. Lett. B **636**, 40 (2006).

[14] S. Ostapchenko, Phys. Rev. D **77** (2008) 034009.

[15] T. Pierog and K. Werner, astro-ph/0611311.

[16] P. Grieder, Proc. of 13-th Conf. on Cosmic Rays (Denver), v. 4, p. 2467, 1973.

[17] T. Antoni *et al.* (KASCADE Collab.), Astopart. Phys. **24** (2005) 1.

[18] R. U. Abbasi *et al.* (HiRes Collab.), Astroph. J. **622** (2005) 910.

[19] M. Unger *et al.* (Pierre Auger Collab.), in Proc. of 30-th Int. Cosmic Ray Conf. (Merida, Yucatan), 2007; astro-ph/0706.1495.

[20] V. de Souza *et al.* (KASCADE-Grande Collab.), in Proc. of 30-th Int. Cosmic Ray Conf. (Merida, Yucatan), 2007.

[21] V. S. Berezinsky and S. I. Grigorieva, Astron. Astroph. **199** (1988) 1.

[22] R. Aloisio *et al.*, Phys. Rev. D **77** (2008) 025007.

[23] R. Engel *et al.* (Pierre Auger Collab.), in Proc. of 30-th Int. Cosmic Ray Conf. (Merida, Yucatan), 2007.

[24] J. Jalilian-Marian *et al.*, Nucl. Phys. B **504** (1997) 415; E. Ianku, A. Leonidov and L. Mclerran, Nucl. Phys. A **692** (2001) 583.